Opt Quant Electron (2017) 49:152
DOI 10.1007/s11082-017-0992-9

CrossMark

Effects of nonuniform distribution of quantum well and quantum wire base on infrared photodetectors under dark conditions

Mohamed S. El_Tokhy[1] · Imbaby I. Mahmoud[1]

Received: 14 December 2016 / Accepted: 15 March 2017 / Published online: 20 March 2017
© Springer Science+Business Media New York 2017

Abstract This paper presents the effects of uniformity and nonuniformity distribution of quantum well (QW) and wire (QR) base on quantum infrared photodetectors under dark conditions. These detectors are quantum well infrared photodetectors (QWIP) and quantum wire infrared photodetectors (QRIP). Analytical expressions for dark current characteristics of the considered devices are implemented. Additionally, the proposed results are validated against published results in literature and high agreement is accomplished. The potential distribution in QWIP active region depends on weak non-locality approach. Also, the effect of electrons concentration above the barriers on the performance of QRIP is considered. The nonuniformity parameter of QRIP is computed. Moreover, the uniformity and nonuniformity distributions effects of QRs and QWs on dark current ratio between QRIP and QWIP are estimated. This current ratio is changed by uniformity and nonuniformity distribution of QWs and QRs. It is noted that dark current ratio between QRIP and QWIP decreases with applied bias voltage. Hence, the QWIP device is affected by applied bias voltage greater than QRIP. However, this current ratio increases with temperature. Accordingly, the QRIP device is influenced by temperature larger than QWIP. It is noticed that dark current ratio under uniformity distribution is smaller than this ratio under nonuniformity distribution for both QRs and QWs. So, the nonuniformity problem within QRs is a great challenge that must be addressed. Also, the nonuniformity distribution introduces limits to QRIP device characteristics. The results demonstrate that zero value of dark current ratio is attained with zero value of nonuniformity parameter. Also, the dark current of QRIPs is found to be greater than of QWIP structures under large variation of nonuniformity distribution. Even though, this parameter is approximated to 1 under uniform distribution of QWs and QRs. It is observed that nonuniformity distribution parameter is vanished up to 80 K. So, the dependence of the operating temperature on the number of electrons occupied by each QR is evaluated. The obtained results confirm that the applied bias voltage decreases this challenge to some extent. Besides, parameters

✉ Mohamed S. El_Tokhy
engtokhy@gmail.com

[1] Engineering Department, NRC, Atomic Energy Authority, P. No. 13759, Inshas, Egypt

optimization for QWIPs and QRIP is of primary concern. Therefore, the devices performance is improved. Consequently, the operations of underlined infrared photodetectors are robust against noise sources in far infrared spectrum.

Keywords Night vision · Optoelectronic · Imaging · Nanoscale · Signal to noise ratio (SNR)

1 Introduction

Recently, quantum infrared photodetectors have been the focus of much attention due to its potential use in far infrared (FIR) (Etteh and Harrison 2001). Extending wavelength range of these detectors into (30–300 μm or 10–1 THz) this region of the infrared (IR) spectrum (Etteh and Harrison 2003) would be beneficial in the fields of defense, satellite mapping and astronomy compared to their currently used counterparts such as Ge and thermal detectors (Etteh and Harrison 2001). Infrared (IR) photodetectors are essential for the variety of applications, including earth resources, medical, targeting and tracking, night vision, energy conservation and industry applications (Liu et al. 2015). A quantum well (QW) structure designed to detect IR light is commonly referred to as a quantum well infrared photodetector (QWIP) (Gunapala et al. 2007). QWIP are first demonstrated in 1987 and still remain as a topic of high scientific interest (Gunapala et al. 2009; Goldberg et al. 2005; DeCuir et al. 2015). QWIPs have been widely investigated for detection in the long wave IR (8–14) μm region of the spectrum (Guériaux et al. 2009). Moreover, the main commercial applications of QWIPs are devoted for imagery in both atmospheric transparency windows (3–5) and (8–12) μm. However, the recent defense and aerospace issues have rapidly raised the interest for the maturity of devices operating in the (12–20) μm wavelength region (Castellano et al. 2009). The expansion of the operating wavelength of the QWIP into this terahertz gap (or the FIR region) is inhibited by the noise source of QWIPs that called the dark current. This current flows in the device in the absence of incident photons (Etteh and Harrison 2003). The dark current in quantum photodetectors is one of the most important parameters that limits its operation at elevated temperatures and decides the detector noise (Negi and Kumar 2015). Compared with QW structures, quantum wire (QR) materials supply additional possibilities for managing photoelectron lifetime and optoelectronic characteristics through manipulation of electron processes in wires (Mitin et al. 2013). Quantum wire infrared photodetectors (QRIPs) utilizing intersubband transitions inside QRs are commonly known to be of great promise for the thermal imaging with high operating temperature (Ling et al. 2009). In recent years, QRIP devices have been attracting much interest (Matsukura et al. 2009). Since, they are expected to surpass conventional and well developed QWIPs.

These two dimensional confinement of the QR structure provides the potential to overcome the electron phonon interaction and relax the selection rule of intersubband transition in QW structures (Ling et al. 2009; Wang et al. 2009). Hence, QRIPs are of great possibility to surpass the drawbacks of commercialized QWIPs. Since, they become low cost and high temperature operation IR detectors (Wang et al. 2009; Gunapala et al. 2007). Moreover, the two dimensional confinement of the nanoscale QRs allows normal incidence absorption by altering the optical transition selection rule. Also, the photoexcited carrier lifetime increases by reducing optical phonon scattering through the ‘‘phonon bottleneck’’

mechanism (Gunapala et al. 2007). Therefore, QRIPs provide increased performance over existing QWIP (Gunapala et al. 2007). Conversely, QRIP devices stated in the literature have not been as good as expected. Signal to noise (SN) is one of the important characteristics of an IR detector such as noise equivalent temperature difference (Matsukura et al. 2009).

In a conventional QWIP structure, the same QW and barriers are repeated. Hence, the absorption region is generally considered as a uniform active region. Recently, some studies have revealed that the QWs cannot be treated the same. A self-consistent model has proven that the electric field distribution in the QW region is nonuniform. This electric field in the first few barriers is much higher than that in the rest of the region. Consequently, the electric field distribution can greatly change the characteristics of QWIPs (Ershov et al. 2000). A nonuniformity QW base is used in QWIP to alter the distribution of the electric field. The barrier width and doping concentration is not the same for all the QWs in this structure. So, lower dark current and higher gains can be achieved with the improvement of nonuniformity distribution of QWIP devices (Wang et al. 2001; Wang and Lee 2000). Similarly, the nonuniform dopant incorporation adversely affects the performance of the QRIP (Martyniuk and Rogalski 2008). Thus, improving QR uniformity is a key issue in the increasing absorption coefficient and enhancing the performance. Therefore, the growth and design of unique QR heterostructure is one of the most important issues related to achievement of state-of-the art QRIP performance (Wang et al. 2001; Wang and Lee 2000). The QRIP performance reduced due to both the nonoptimal band structure and nonuniformity in QR size. On other hand, the reduced optical absorption in QRs due to size nonuniformity increases the normalized dark current. Moreover, the BLIP temperature of QRIP is strongly depends on nonuniformity of the QR size (Martyniuk and Rogalski 2008).

The dark current is the commonly known noise source of these photodetectors (El_Tokhy and Mahmoud 2015). It inhibits the correct detection of these low-level signals. A great deal of research has gone into the removal of this noise source in QWIPs/QRIPs. Practically, efforts are usually limited to cooling of the device (Etteh and Harrison 2001). Also, dark current determines the signal to noise ratio (SNR) and the maximum operation temperature of QWIPs and QRIPs. Thus, it is important to minimize this current during the device design. The reduction of dark current plays a fundamental role on the optimization of photodetectors. Consequently, it demands a generalized model that able to reproduce experimental data for structures with different band-edge potentials (de Moura Pedroso et al. 2017). A theoretical dark current analysis may be used to study and evaluate the characteristics of the QWIPs/QRIPs in order to enhance design parameters of these devices under nonuniformity distribution of QW/QR base (Liu et al. 2015). The paper is organized as follows: the basic assumption and operational principles are described in Sect. 2. Section 3 shows the dark current analysis of quantum infrared photodetectors under effects of nonuniformity distribution of QW/QRs base. The main numerical results obtained with their discussion are presented in Sect. 4. Section 5 is devoted to conclusion of the work.

2 Basic assumptions and operational principles

The QWIP is a semiconductor device that commonly made of thin layers of gallium arsenide (GaAs) alternated to layers of aluminium gallium arsenide (AlGaAs) (Meola et al. 2015; Altin et al. 2013). The GaAs/AlGaAs QW devices have a number of promising

advantages such as high yield and thus low cost, the use of standard manufacturing techniques based on mature GaAs growth and processing technologies. Also, it has extrinsic radiation hardness with well-controlled molecular beam epitaxy (MBE) growth on GaAs wafers (Meola et al. 2015). Thus, processing and growth technologies of GaAs structures lead to reproducibility. Accordingly, large area and low cost detector arrays are achieved (Altin et al. 2013). But, the QWIPs present some problems such as lower operating temperature, low quantum efficiency, complex light coupling schemes, high dark currents and narrow spectral response that limit sensitivity in low background conditions. One of the drawbacks is that photons normally impinging are not absorbed. Consequently, the so roughed surfaces are needed to scatter photons inside the detector (Meola et al. 2015). On other hand, a widely claimed advantage for QWIPs is the band gap engineering. Moreover, the versatility of the III–V processing allowing the custom design of quantum structures in order to detect in a large spectral range (Guériaux et al. 2009). One major problem of these devices is electron transport in the dark conditions (Guériaux et al. 2009). The three components of the dark current are the ground state sequential tunneling, the thermally assisted tunneling and the thermionic emission as shown in Fig. 1a (Etteh and Harrison 2003). The electrons scattering from the localized state in one QW into the next describes the sequential tunneling component. The thermally assisted tunneling component compromises thermalised carriers in the higher momentum states of the QW tunneling via the barrier tip and into the continuum (de Moura Pedroso et al. 2017). Finally, the thermionic emission component refers to the excitation of carriers from the well and into the continuum as illustrated in Fig. 1b (El_Tokhy et al. 2010). These processes take place under the effect of an applied field. Hence, the carriers will constitute a dark current due to once in the continuum (Etteh and Harrison 2003).

The QW represents the base of QWIP structures. Hence, the QW structure plays a role of the photodetector base. However, the base of the proposed QRIP consists of an array of QRs in contrast with QWIPs.

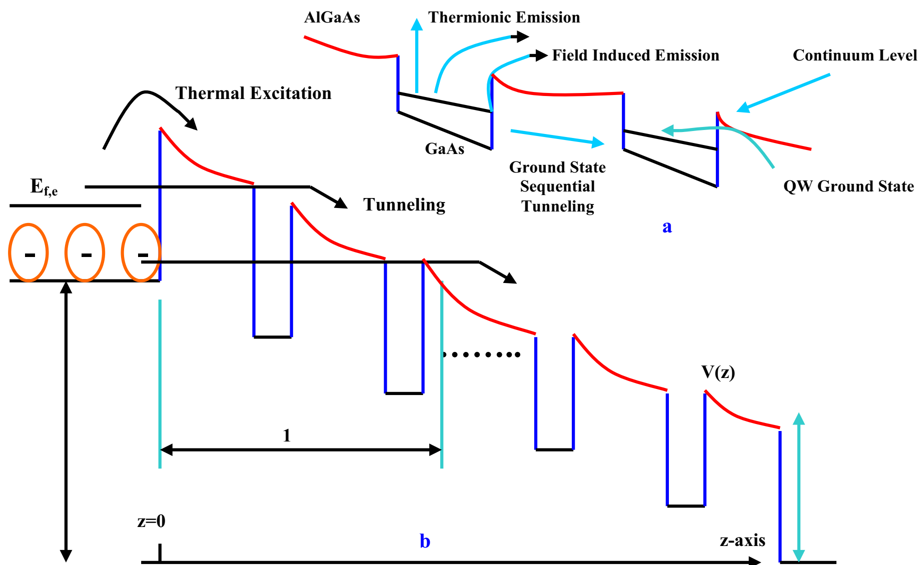

Fig. 1 Dark current models, *a* three mechanisms of the dark current, *b* thermionic emission and tunneling from the emitter to the QWIP region

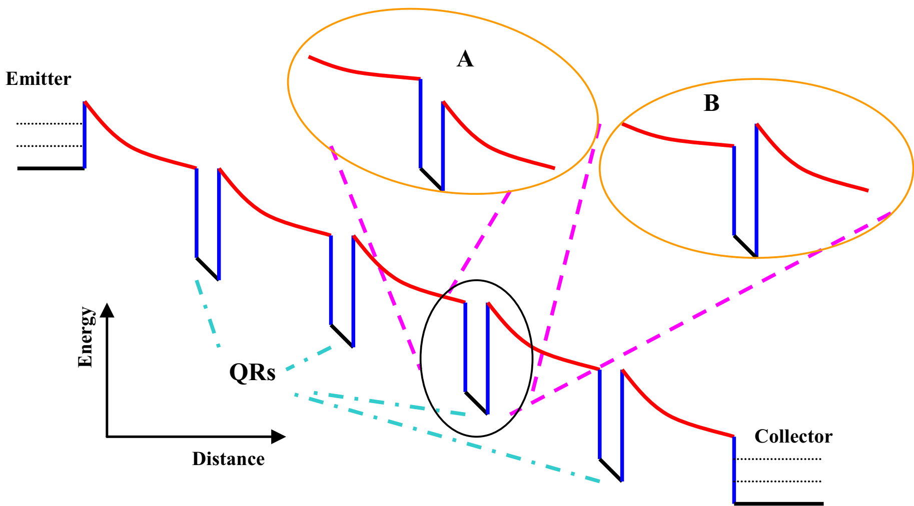

Fig. 2 The conduction band profile of QRIP and forms of QRs with different asymmetric distributions of donors (*A* and *B*)

The QRIP is mainly consists of barrier layers of excited regions and repetitive QR composite layers (Bai et al. 2013). The conduction band profile of nonuniformity QRIP is shown in Fig. 2 (Ryzhii et al. 1999). This figure shows that adjacent QRs have different asymmetric distributions of donors. A QRIP device is mainly comprised of active regions, top contact and bottom contact. The active region is a multiple two dimensional array of QRs separated by barriers. Moreover, it is sandwiched between top and bottom contacts (Liu et al. 2013, 2015). The top and bottom contacts are utilized as the emitter and collector, respectively. The incident IR light is absorbed in the active regions. It results in electrons intraband transitions that may be sub-band to sub-band or sub-band to continuum transitions. The injected electrons from the emitter may be captured by QRs. Furthermore, these electrons may be drifted toward the collector under applied electrical field (Liu et al. 2015). Each QR layer is mainly consists of many periodically distributed QRs. Also, the lateral size of QRs is assumed to be large enough. Therefore, each QR has a large number of bound states to accept more electrons (Liu et al. 2013). Though, the transverse size of QRs is smaller than the distance between the QRs layers in order to be provided with single energy level related to the quantization in this direction (Liu et al. 2013).

3 Dark current analysis of quantum infrared photodetectors

3.1 Dark current of QWIPs under uniform and nonuniform distribution of QWs

The potential distribution in QWs is obtained from the solution of commonly known Poisson equation. It needs a 3D treatment involving numerical solution of Poisson equation. It is assumed that the variation of sheet donor density, $\delta\Sigma_d = \Sigma_d - \langle\delta\Sigma_d\rangle$, is small ($|\Sigma_d| \ll \langle\Sigma_d\rangle$) and uncorrelated in case of random fluctuations of the sheet donor density in the QW. Therefore, the Gaussian statistics is used to find the probability, w, of the

formation of fluctuations as $w \sim e^{-\lambda\langle\Sigma_d\rangle\left(\frac{\delta\Sigma_d}{\langle\Sigma_d\rangle}\right)^2}$ (Ryzhii et al. 1995). The two dimensional character of the random distribution of the donors in the QW is considered. Hence, the fluctuations is taken into account when $\lambda^2 = \mathrm{W_e W_c}$ (W_c and W_e are the thicknesses of the collector and the emitter, respectively). Thus, the shorter fluctuations of the donor density lead to a relatively smooth distribution of the potential in the QW plane. So, smaller variations of the electron density are achieved. Then, a lower estimate of the nonuniformity quantity (ψ) is obtained with ignoring very short fluctuations (Ryzhii et al. 1995). The exponential dependence of ψ on the fluctuations of the potential (φ) leads to optimal fluctuations (Ryzhii et al. 1995). Consequently, the electric field can be effectively nonuniform but rather smooth with a scale of nonuniformity (λ) comparable to the QW structure thickness (Ryzhii and Liu 1999). The case of relatively long fluctuations of the sheet electron density is supposed when the scale of the nonuniformity (λ) achieves the inequality $\lambda > \sqrt{\mathrm{W_e W_c}}$. Furthermore, it is preferable to use the weak non-locality approach. Hence, the QW potential ($\varphi = \varphi(y, z)$) achieves the subsequent formula in this approach (Ryzhii et al. 1995)

$$\frac{W_e + W_c}{3}\left(\frac{\partial^2\varphi}{\partial y^2} + \frac{\partial^2\varphi}{\partial z^2}\right) - \frac{\varphi}{W_e} + \frac{V - \varphi}{W_c} = \frac{4\pi q}{\text{æ}}(\Sigma - \Sigma_0) \tag{1}$$

where æ, q, Σ, Σ_0, V and φ denote the permittivity of the lattice, the electron charge, the sheet electron density in the QW, the sheet electron density in the QW in equilibrium, bias voltage and the potential of QW, respectively. The sheet electron density (Σ_0) in the QW at equilibrium is described by

$$\Sigma_0 = \Sigma_d + \frac{(W_e + W_c)}{1 + a_B(W_e + W_c)}\left(\frac{\text{æ}}{\pi q}\left(\varepsilon_i + \varepsilon_f\right) - a_B\langle\Sigma_d\rangle\right) \tag{2}$$

where m^*, ε_f, a_B, $\hbar$, ε_i, Σ_d and $< >$ denote the effective electron mass, the Fermi energy in the contact region, the Bohr radius that given by $a_B = \frac{\text{æ}\hbar}{m^* q^2}$, the reduced Planck constant, the ionization energy (the energy of excitation of electrons out of the QW), the sheet donor density in the QW and the means averaging over the plane of QWs, respectively. Equation (1) is supposed for nonuniformity of the dopant distribution in the plane of the QWs. The density of the donors in the QW plane is considered to have a maximum in the centre of the QW with a general form stated as

$$\Sigma_d(z) = \langle\Sigma_d\rangle\left(1 + \Delta\cos\left(\frac{\pi z}{L}\right)\right) \tag{3}$$

where Δ is a parameter ($0 \le \Delta \le 1$) and $L = L_y = L_z$. Consequently, the uniform dopants distribution of the QWs ($y = 0$) takes the following formula (El_Tokhy et al. 2010)

$$\frac{W_e + W_c}{3}\frac{\partial^2\varphi}{\partial z^2} - \frac{\varphi}{W_e} + \frac{V - \varphi}{W_c} = \frac{4\pi q}{\text{æ}}(\Sigma - \Sigma_0) \tag{4}$$

The boundary conditions for solving Eq. (4) are considered as

$$\varphi|_{z=0} = 0 \quad \text{and} \quad \varphi\big|_{z=(M+1)L} = V \tag{5}$$

where z, M and V denote the width of the active region ($0 \le z \le (M + 1)L$), the number of quantum wells and the applied voltage, respectively. A formula for the potential

distribution within QWs is deduced and modified by solving Eq. (4) with boundary conditions of Eq. (5) that yields

$$\varphi(z) = \frac{1}{æLqA_1}\left(\alpha + 12L^2\pi q^2\Sigma\Delta W_e W_c \cos\left(\frac{\pi z}{L}\right)\mathrm{X} - \frac{\Theta W_e W_c}{\Omega}\psi - \frac{1}{\prod}\left(3\gamma L^2 W_e^2(4W_c + a_B) - \gamma W_e W_c \wp\right)\right) \tag{6}$$

where $\mathrm{X} = (W_e W_c + W_c a_B + W_e a_B)$, $h_d = \frac{2\pi q \Sigma_d}{æ}$, $\alpha = \frac{J_m P_c}{q h_d}$, $\psi = \left(\wp + 3L^2 a_B \frac{W_e}{W_c}\right)$, $\wp = \left(2\pi^2 W_e W_c(a_B + 2W_c + W_e) + 12L^2(W_c + W_e) + \pi^2 a_B\left(W_e^2 + W_c^2\right) + 3L^2 a_B\left(\frac{W_c}{W_e} + 1\right)\right)$, $A_1 = (6L^2 W_c W_e\ (2W_e + 2W_c + a_B) + 3L^2 a_B\ (W_e^2 + W_c^2) + \pi^2 W_e W_c A_3)$, $A_3 = 4W_e W_c + W_c a_B + W_e a_B$, J_m is the maximum current density from the emitter that based on the doping level of the emitter and P_c represents the probability of electron capture into the QW. In addition, the emitter (E_e) and collector (E_c) electric fields are the integral characteristics of the electron distribution over the QWs. Therefore, an expression for the emitter electric field is introduced by manipulation of Eq. (4) with boundary conditions of Eq. (5) as (El_Tokhy et al. 2010)

$$E_e = \frac{\partial\varphi}{\partial z}\Big|_{z=0} \tag{7}$$

The absolute value of the electric field is presented at emitter barrier with $z = 0$. Also, it corresponds to the plane between the extreme barrier and emitter contact layer. Hence, the common known formula Eq. (7) is strict with the average normalized electron sheet concentration. The differentiation of Eq. (6) with respect to z is performed. Therefore, a formula for emitter electric field is obtained and modified by substitution from Eq. (6) in Eq. (7) as

$$E_e = \frac{\kappa\sqrt{3}\sqrt{W_e W_c}(\zeta A_{51} - A_1 A_{51})}{æ\zeta LqA_1^2\left(A_4^2 - 1\right)} \tag{8}$$

where $\kappa = \pi^2\ (W_c + W_e)\ A_3 + 3L^2\ (4\ (W_e + W_c) + a_B\ (W_e + W_c) + 2a_B)$, $\Gamma = A_4 A_{49}$, $\zeta = (W_e + W_c)(\pi^2 W_e W_c + 3L^2)$, $A_{49} = \exp\left(-L\sqrt{\frac{3}{W_e W_c}}\right)$, $A_4 = \pi W_e^3 W_c^2 E æ L A_3$ and A_{51} denotes a set of parameters. The dark current density represents the current flowing via the detector if there is no incident radiation that divided by the metal contact area (El_Tokhy and Mahmoud 2014; Kuffner 2006). Furthermore, dark current is one of the most significant parameters that degrade the performance of an IR photodetector. It is a source of noise (Kuffner 2006). Moreover, it is the major limiting factor of the detector's performance at much higher temperatures (de Moura Pedroso et al. 2017; Altin et al. 2013; Bai et al. 2013; Soibel et al. 2009). Thus, the QWIP detectors have to be cooled in the range of 50–77 K to decrease this current. Hence, the cost of a commercial photodetector is raised (Hansson and Rachavula 2006). The density of the electron tunneling current injected through the emitter barrier to the QW structure is stated as (Ryzhii and Liu 1999; Ryzhii et al. 2000b; Ryzhii and Ryzhii 2000)

$$\mathrm{J_{dark}} = \mathrm{J_m}\exp\left(-\frac{\mathrm{E_t}}{\mathrm{E_e}}\right) \tag{9}$$

where $\mathrm{E_t}$ is the characteristic tunneling field. The substitution from Eq. (8) into Eq. (9) yields

$$\mathrm{J_{dark}} = \mathrm{J_m}\exp\left(\frac{æLqA_1^2\mathrm{E_t}\left(A_4^2-1\right)\zeta}{\kappa\sqrt{3}\sqrt{W_eW_c}(\Gamma A_1 - A_{51}\zeta)}\right) \tag{10}$$

However, the density of the electron tunneling current can be expressed as (Ryzhii 1997)

$$\mathrm{J_{dark}} = \frac{\mathrm{J_m}}{\alpha}\exp(\eta_d(\Theta - 1)) \tag{11}$$

where Θ and η_d represent the average normalized electron sheet concentration ($\Theta = \frac{\Sigma}{\Sigma_d}$) and the rate of the electron thermo-excitation from the QW if $\Sigma_n = \Sigma_d$ ($\eta_d = \frac{\pi\hbar^2\Sigma_d}{m^* K_B T}$, where K_B and T denote Boltzmann constant and the temperature, respectively). A different treatment is applied to obtain the parameter Θ than that in (Ryzhii 1997). An expression for Θ is introduced by handling between Eqs. (10) and (11).

$$\Theta = \frac{1}{2}\left(\Lambda + \sqrt{\left((\Lambda)^2 + 4b_9\left(1 + \frac{\ln(\alpha)}{\eta_d b_8}\right)\right)}\right) \tag{12}$$

where $b_1 = \frac{(M+1)L\sqrt{3}\sqrt{W_eW_c}}{W_eW_c}$, $b_2 = \pi q^2\Sigma W_c^2W_e^2L^2 \exp(b_1)$, $b_3 = \pi^3q^2\Sigma W_c^3W_e^3$, $b_4 = \pi q^2\Sigma W_c^2W_e^2L^2$, $b_5 = \pi^3q^2\Sigma W_c^3W_e^3 \exp(b_1)$, $b_6 = \pi^3q^2\Sigma W_c^3W_e^3 \exp(2b_1)$, $b_7 = L^2\pi q^2\Sigma W_c^2 W_e^2 \exp(2b_1)$, b_8 is defined as a set of parameters, $b_9 = \left(\begin{array}{l}16(3A_1 + A_2 + 3A_4) + 12L_2W_eW_c\pi q^2\Sigma\Delta\times \\ (a(W_e + W_c) + 4W_eW_c + \exp(2A_3)(W_e + W_c(5 + 12W_e)))\end{array}\right)$ and $\Lambda = \left(1 + \frac{\ln(\alpha)}{\eta_d} - \frac{b_9}{b_8} - \frac{1}{3\eta_d b_8}\left(qæ\sqrt{W_c}E_t\sqrt{3}\zeta(-1 + \exp(2b_1)A_3)\right)\right)$. Furthermore, an expression for dark current density can be described by (Ryzhii 1997)

$$\mathrm{J_{dark}} = \frac{\mathrm{qh_d}}{\mathrm{P_c}}\exp(\eta_d(\Theta - 1)) \tag{13}$$

A closed form expression for dark current density is introduced by substitution from Eq. (12) into Eq. (13) that modified and rewritten as

$$\mathrm{J_{dark}} = \frac{\mathrm{qh_d}}{\mathrm{P_c}}\exp\left(\frac{\eta_d}{2}\left(\Lambda - 1 + \sqrt{\left((\Lambda)^2 + 4b_9\left(1 + \frac{\ln(\alpha)}{\eta_d b_8}\right)\right)}\right)\right) \tag{14}$$

3.2 Dark current of QRIPs under uniform and nonuniform distribution of QRs

This paper addresses the optical properties of QRIP with a different manner to that in (El_Tokhy et al. 2010; Barickaby et al. 2011; Ryzhii et al. 1996). The proposed models take into account the nonuniformity distribution parameter of QRs base in QRIPs. To the knowledge of the authors, the effect of this parameter on the dark current of QRIP does not considered before in the literature. Consequently, the effect of QRs distribution on the device performance is the primary scope in the current paper. Also, the possibilities of overcoming the consequences of this parameter on dark current are investigated. Moreover, the device performance under QR nonuniformity distribution is compared and analyzed with uniformity distribution of QRs.

3.2.1 Effects of nonuniformity distribution of QRs on QRIP performance

The z-coordinate corresponds to the vertical direction on the QR layer plane. However, x and y are the in-plane coordinates. The average potential is illustrated by Poisson equation. Since, the space charge is averaged in the in-plane directions. Therefore, the average potential Poisson equation can be given by (Ryzhii et al. 2000a, b; Ryzhii and Ryzhii 2000)

$$\frac{d^2\langle\varphi\rangle}{dz^2} = \frac{4\pi q}{æ}\sum_{k=1}^{M}\left(\langle N\rangle\Sigma_{QR} - \rho_D + \rho\right)\delta(z - kL) \tag{15}$$

where δ(z), q, M, Σ_{QR}, æ, ρ_D, ρ, L, <N> and φ denote Dirac delta function, the electron charge, the total number of the QR layers, the density of QRs arrays, the donor density of QRs arrays, dielectric constant of the material from which the QR is fabricated, the concentration of electrons above the barriers, the transverse spacing between QRs, the average extra carrier number in the QRs (the symbol <…> means averaging over the base plane) and the potential in the QR base plane, respectively. Equation (15) can be solved using the next boundary condition as

$$\varphi = \begin{cases} 0 & \text{at} \quad z = 0 \quad (At\, the\, emitter) \\ V & \text{at} \quad z = (M+1)L \quad (At\, the\, collector) \end{cases} \tag{16}$$

where V represents the applied bias voltage. Consequently, a formula for the average potential is deduced and simplified as

$$\langle\varphi\rangle = C_5 Z - Z^2\frac{(2C_5L - 2V + 2C_5LM)}{2L^2M^2 + 4L^2M + 2L^2} \tag{17}$$

where C_5 denotes the set of solution. Also, the potential in the QR base plane is stated as (El_Tokhy et al. 2010)

$$\varphi = \frac{4\sqrt{2}}{æ}\langle N\rangle q\sqrt{\Sigma_{QR}}\left(\Delta - \frac{1}{2}\Sigma_{QR}\left(x^2 + y^2\right)\right) \tag{18}$$

Conversely, the potential variation can be stated as

$$\delta\varphi = \varphi - \langle\varphi\rangle \tag{19}$$

Hence, an equation for the variation of potential is obtained by substitution from Eqs. 17–18 into Eq. 19 that yields

$$\delta\varphi = \left\{\frac{4\sqrt{2}}{æ}\langle N\rangle q\sqrt{\Sigma_{QR}}\left(\Delta - \frac{1}{2}\Sigma_{QR}\left(x^2 + y^2\right)\right) - C_5Z + Z^2\frac{(2C_5L - 2V + 2C_5LM)}{2L^2M^2 + 4L^2M + 2L^2}\right\} \tag{20}$$

The numerical value for the average extra carrier number in the QRs is the primary issue to find. Consequently, a different manner is manipulated depending on capture probability (P_c) of the carriers passing through QRs. It can be approximated by (El_Tokhy et al. 2010; El_Tokhy et al. 2009)

$$P_c = P_o\frac{(N_{QR} - \langle N\rangle)}{N_{QR}}e^{-\frac{q^2\langle N\rangle}{CK_BT}} \tag{21}$$

where K_B, C, P_o, N_{QR}, a_{QR} and T denote the Boltzmann constant, the capacitor of the QR, the capture probability under neutral condition, the maximum electron number

that a QR can accommodate, lateral characteristic size of QR and the temperature, respectively. Though, the capacitor of the QR can be given by (El_Tokhy et al. 2010)

$$C = \frac{2æa_{QR}}{\pi\sqrt{\pi}} \tag{22}$$

A closed form expression for the average number of carrier in the QRs is proposed by solving Eq. (21) that simplified and yields

$$\langle N\rangle = \frac{-2æa_{QR}K_BT}{\pi\sqrt{\pi}q^2} Lambertw\left(\frac{1}{2}\frac{\pi\sqrt{\pi}q^2N_{QR}P_c e^{\frac{1}{2}\frac{\pi\sqrt{\pi}q^2N_{QR}}{æa_{QR}K_BT}}}{P_o æa_{QR}KBT}\right) + N_{QR} \tag{23}$$

This formula is obtained with a different manner to that in (Barickaby et al. 2011). Therefore, a formula for the potential variation is introduced by substitution from Eq. 23 into Eq. 20. The sheet electron density in the QR base is assumed to be a periodic function because of the periodicity of the QR array. The potential distribution within QRIP structure under nonuniformity distribution of QRs is described by Eq. (19). Hence, the nonuniformity parameter of QRIP is specified by (Ryzhii et al. 1996)

$$\psi = \left\langle e^{\frac{q\delta\varphi}{kT}}\right\rangle \tag{24}$$

The average notation in the right hand side of Eq. (24) is simplified. It is manipulated to be as follows

$$\psi \approx \frac{1}{\left(\frac{L_{QR}}{2} - \left(-\frac{L_{QR}}{2}\right)\right) \times \left(\frac{l_{qr}}{2} - \left(-\frac{l_{qr}}{2}\right)\right)} \int_{-\frac{l_{qr}}{2}}^{\frac{l_{qr}}{2}} \int_{-\frac{L_{QR}}{2}}^{\frac{L_{QR}}{2}} e^{\frac{q\delta\varphi}{K_BT}} dxdy \approx \frac{1}{L_{QR} \times l_{qr}} \int_{-\frac{l_{qr}}{2}}^{\frac{l_{qr}}{2}} \int_{-\frac{L_{QR}}{2}}^{\frac{L_{QR}}{2}} e^{\frac{q\delta\varphi}{K_BT}} dxdy \tag{25}$$

where L_{QR} and l_{qr} denote the longitudinal length size of each QRs and lateral size of each QRs, respectively. This expression represents the integration of fluctuation of exponential potential field distribution within QR base. This integration is done in the growth direction of QRs over x- and y-directions. However, the longitudinal length size of each QR corresponds to 1/20 of the lateral size of each QR (Barickaby et al. 2011). Thus, the nonuniformity (ψ) distribution of QR base within their QRIP structure is demonstrated by (Barickaby et al. 2011)

$$\psi \approx \frac{1}{L_{QR} \times \frac{1}{20} L_{QR}} \int_{-\frac{L_{QR}}{2\times 20}}^{\frac{L_{QR}}{2\times 20}} \int_{-\frac{L_{QR}}{2}}^{\frac{L_{QR}}{2}} e^{\frac{q\delta\varphi}{K_BT}} dxdy \approx \frac{20}{L_{QR}^2} \int_{-\frac{L_{QR}}{40}}^{\frac{L_{QR}}{40}} \int_{-\frac{L_{QR}}{2}}^{\frac{L_{QR}}{2}} e^{\frac{q\delta\varphi}{K_BT}} dxdy \tag{26}$$

This double integral in Eq. (26) is simplified after substitution from Eq. (20) in Eq. (26). A closed form expression for the nonuniformity parameter distribution of QR base is proposed that simplified as

$$\psi = \frac{\xi\pi e^{\frac{4\sqrt{2}\sqrt{\Sigma_{QR}}\lambda_1}{\lambda_2}} e^{\vartheta} erf\left(L_{QR}\sqrt{-2\sqrt{2}\Sigma_{QR}^{3/2}\lambda_7/\lambda_2}\right) erf\left(5L_{QR}\sqrt{-2\sqrt{2}\Sigma_{QR}^{3/2}\lambda_8/\lambda_2}\right)}{L_{QR}^2 e^{\frac{\lambda_{10}}{K_B\pi^{3/2}Tq^2}}\sqrt{-\Sigma_{QR}^{3/2}\lambda_{11}/\lambda_2}\sqrt{-2\sqrt{2}\Sigma_{QR}^{3/2}\lambda_{12}/\lambda_2}} \tag{27}$$

where $\vartheta = \frac{\lambda_3}{\lambda_4} + \frac{\lambda_5}{\lambda_6} - \frac{\lambda_9}{\lambda_6}$, $\xi = 0.029$ and $\lambda_2 = K_B\pi^{3/2}T æ$.

3.2.2 Effects of nonuniformity distribution on dark current ratio between QRIP and QWIR

The dark current ratio (J_d^{QRIP}/J_d^{QWIP}) between QRIP and QWIP is estimated. The sources of dark current in QRIP are assumed to include field-assisted tunneling emission from QRs, thermal generation of carriers and thermionic emission from QRs. The average electron sheet density for the undoped QR base is evaluated and yields (Ryzhii et al. 1995)

$$\Sigma_i = \frac{æ}{4\pi q^2}\left(\frac{W_c + W_e}{W_c W_e}\right)\left(\varepsilon_i + \varepsilon_f\right), \quad \langle\Sigma\rangle \cong \Sigma_i + \frac{æV}{4\pi q^2 W_c} \tag{28}$$

where ε_i, ε_f, W_c, W_e and $\langle\Sigma\rangle$ denote the ionization energy of the quantum level in the QR, the Fermi energy of the electrons in the emitter and collector regions, the thicknesses of the collector N regions, the thicknesses of the emitter and average electron sheet density, respectively. The dark current ratio between QRIP and QWIP depends on the same average sheet electron density. This current ratio can be described by (Ryzhii et al. 1996)

$$\frac{J_{dark}^{QRIP}}{J_{dark}^{QWIP}} = \psi\left(\frac{1-\beta_{QWIP}}{1-\beta_{QRIP}}\right)e^{\frac{(\pi\hbar a\langle\Sigma\rangle)^2 - 8\pi\hbar^2\langle\Sigma\rangle}{8mK_BT}} \tag{29}$$

where β_{QWIP} and β_{QRIP} denote the efficiency of the electron transport through the QWIP and QRIP, respectively. An expression for the dark current ratio between QRIP and QWIP under nonuniformity distribution of QRs and QWs is proposed by substitution from Eqs. (27–28) into Eq. (29) that modified as

$$\frac{J_{dark}^{QRIP}}{J_{dark}^{QWIP}} = \left(\frac{1-\beta_{QWIP}}{1-\beta_{QRIP}}\frac{\xi\pi\rho e^{\frac{4\sqrt{2}\sqrt{\Sigma_{QR}}\lambda_1}{\lambda_2}} e^{\vartheta} erf\left(L_{QR}\sqrt{-2\sqrt{2}\Sigma_{QR}^{3/2}\lambda_7/\lambda_2}\right) erf\left(5L_{QR}\sqrt{-2\sqrt{2}\Sigma_{QR}^{3/2}\lambda_8/\lambda_2}\right)}{L_{QR}^2 e^{\frac{\lambda_{10}}{K_B\pi^{3/2}Tq^2}}\sqrt{-\Sigma_{QR}^{3/2}\lambda_{11}/\lambda_2}\sqrt{-2\sqrt{2}\Sigma_{QR}^{3/2}\lambda_{12}/\lambda_2}}\right) \tag{30}$$

where $\rho = \exp\left(\frac{1}{8mK_BT}\left(\begin{array}{c}\left(\pi\hbar a\left(\frac{æ}{4\pi q^2}\left(\frac{W_c+W_e}{W_cW_e}\right)\left(\varepsilon_i+\varepsilon_f\right)+\frac{æV}{4\pi q^2 W}\right)\right)^2 \\ -8\pi\hbar^2\left(\frac{æ}{4\pi q^2}\left(\frac{W_c+W_e}{W_cW_e}\right)\left(\varepsilon_i+\varepsilon_f\right)+\frac{æV}{4\pi q^2 W}\right)\end{array}\right)\right)$. Moreover,

the dark current ratio between QRIP and QWIP under uniformity distribution is formulated as

$$\frac{J_{dark}^{QRIP}}{J_{dark}^{QWIP}} = \frac{1-\beta_{QWIP}}{1-\beta_{QRIP}}\rho \tag{31}$$

The above analysis shows a large difference between Eq. (30) that describes nonuniformity distribution of QRs and Eq. (31) of uniformity distribution of QRs.

4 Results and discussion

Explicit solutions for the characteristics of QWIPs and QRIPs structures under nonuniformity distribution of QWs and QRs base are investigated in order to analyze their performances. The parameters values of these devices are depicted in Table 1 (Ryzhii et al. 1996; Li et al. 2007).

4.1 Dark current results of QWIP

The logarithmic change of dark current with bias voltage is depicted in Fig. 3. An agreement between our obtained results with experimental published results (Li et al. 2007) is achieved. The variation of dark current against bias voltage at different spacing between the adjacent wells is shown in Fig. 4. From this figure, the number of thermally excited electrons increases with the bias voltage. Hence, the heating effect is raised with bias voltage. Thus, an increase of the thermionic excitation of electrons into the continuum states is noted. Consequently, an increase of dark current is accomplished. Furthermore, the probability of electrons escaping outside the continuum increases with the spacing between the wells due to tunneling effect. As a result, the dark current increases as shown in Fig. 4. The change of dark current with spacing between QWs at different number of QWs is depicted in Fig. 5. It is observed that the electrons are transport much quickly to the neighbors QWs through the barriers with the number of QWs. Hence, the captures of electrons in the QWs are decreased. Therefore, the dark current increases with the number of QWs. Also, the 3D variation of dark current with bias voltage and temperature is illustrated in Fig. 6. The proposed model result describes the dark current characteristics of QWIPs. Moreover, this model helps in understanding more physical meanings as well as improvements of device performance. These improvements of QWIP were done through device parameters. These parameters are spacing between wells, intensity of incident radiation and number of QW layers. Furthermore, optimizations of these parameters are summarized in Table 2.

The variation of the nonuniformity parameter distribution of QW with the change of bias voltage, operating temperature at different ionizing energy is depicted in Fig. 7. It is

Table 1 QWIP and QRIP parameters (Ryzhii et al. 1996; Li et al. 2007)

QWIP	$\Sigma_d = (0.3–0.6) \times \Sigma$	$a_B = 15$ nm	$W_e = (5–100)$ μm	$\Sigma = 100 \times 10^{12}$ cm^{-2}	$L = (1–40)$ nm
	$m^* = 6 \times 10^{-29}$ g	$æ = 12$	$W_c = (5–100)$ μm	$J_m = 1.6 \times 10^{6}$ A/cm^2	$M = (1–50)$
QRIP	$L_{QR} = (1–100)$ nm	$\beta_{QRIP} = 0.751$	$a_{QR} = (10–40)$ nm	$\varepsilon_i = 100$ MeV	$N_{QR} = 8–10$
	$\beta_{QWIP} = 0.99$	$M = 10$	$T = (80–300)$ K	$\rho = (0.1–4.5) \times 10^{10}$ cm^{-2}	$V = (0–2)$ V

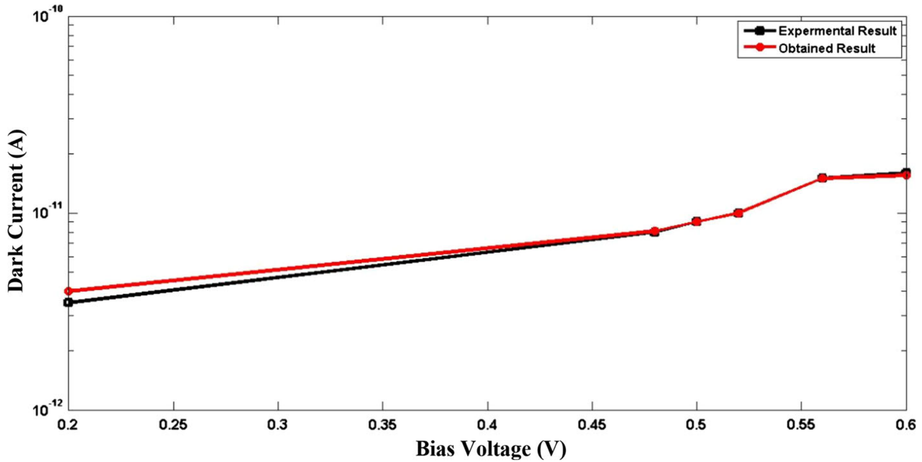

Fig. 3 Dark current of QWIP against bias voltage for comparison between explicit analysis and published results (Li et al. 2007)

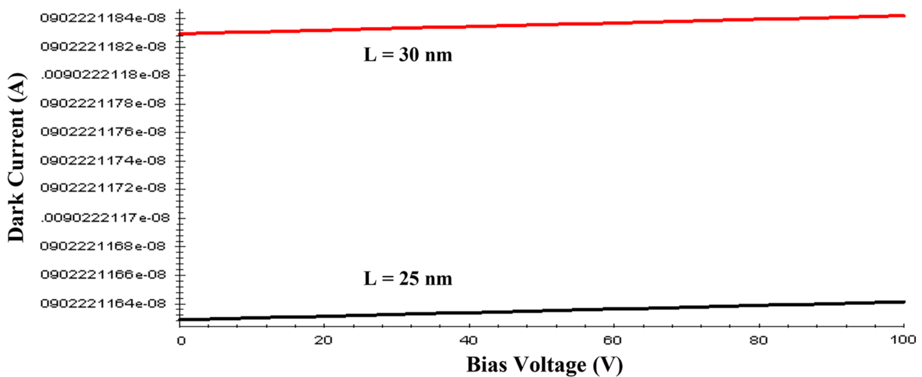

Fig. 4 Dark current against bias voltage at different spacing between QWs with $W_e = 5$, $W_c = 5$ μm, $a_B = 15$ nm, $M = 10$, $\Sigma = 10 \times 10^{12}$ cm^{-2}, $\Delta = 1$ and $T = 150$ K

noted that the potential field applied on QW active region increases with the ionized energy. Hence, variation of the barrier between QW structures is observed. Therefore, the nonuniformity distribution of QW is raised. Another point of observation, the thermal effects of accelerated electrons due to applied bias voltage is increased. Thus, a thermal dissipated energy leads to modification of the potential field distribution within active region of QWIP device. So, the nonuniformity distribution of QWs is increased. Consequently, the nonuniformity effect increases with bias voltage. The effect of ionizing energy and bias voltage at different spacing between QWs on the nonuniformity of QWs is presented in Fig. 8. This figure shows that small variation of nonuniformity distribution is observed with the increase of spacing between QWs.

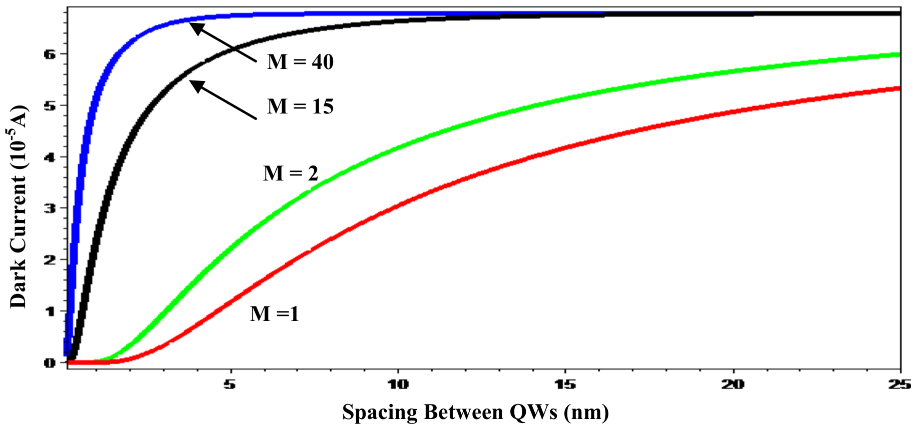

Fig. 5 Dark current against spacing between the QWs at different number of QWs with æ = 12, $W_e = 10$, $W_c = 10$ μm, $\Delta = 0.1$, $J_m = 1.6 \times 10^6$ A/cm^2, $\Sigma = 10 \times 10^{12}$ cm^{-2}, $a_B = 15$ nm, V = 0.9 V and T = 200 K

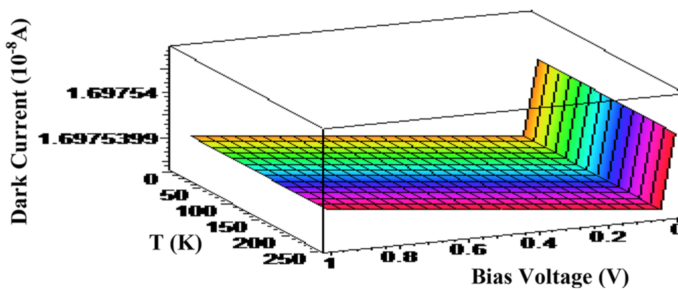

Fig. 6 The 3D relation between dark current against bias voltage and temperature with M = 10, æ = 12, $J_m = 1.6 \times 10^6$ A/cm^2, $W_e = 5$, $W_c = 5$ μm, $\Delta = 1$, $\Sigma = 10 \times 10^{12}$ cm^{-2}, $a_B = 15$ and L = 40 nm

4.2 QRIP numerical results and discussion

4.2.1 Nonuniformity distribution results of QR

The variation of nonuniformity distribution of QR base against number of QR sheet layers at different bias voltage and number of carriers occupied by each QR are depicted in Figs. 9 and 10, respectively. From these figures, the spatial potential distribution within QRIP increases with number of QR sheet layers. This potential field redistributes the QRs within the QRIP structure. Consequently, the nonuniformity distribution of QRs is increased until M = 8. Then, a saturation of the curves is observed that may be due to losses of potential filed within QR puncture. Moreover, the nonuniformity of QRs decreases with the increase of bias voltage as shown in Fig. 9. The applied bias voltage has broken the potential within QRIP active region. Thus, a stream of electrons will travel from the emitter region directed to the collector region. Consequently, the nonuniformity of QRs decreases. However, the small number of electrons within QR increases the nonuniformity of QRs distribution as depicted in Fig. 10. This is may be due to the fact that effect of

Table 2 Optimum values of QWIP parameters

Parameters	Number of QW layers	Separation between wells	$<\Sigma_0>$
Optimum values	10	9.7 nm	0.63×10^{11} cm^{-3}

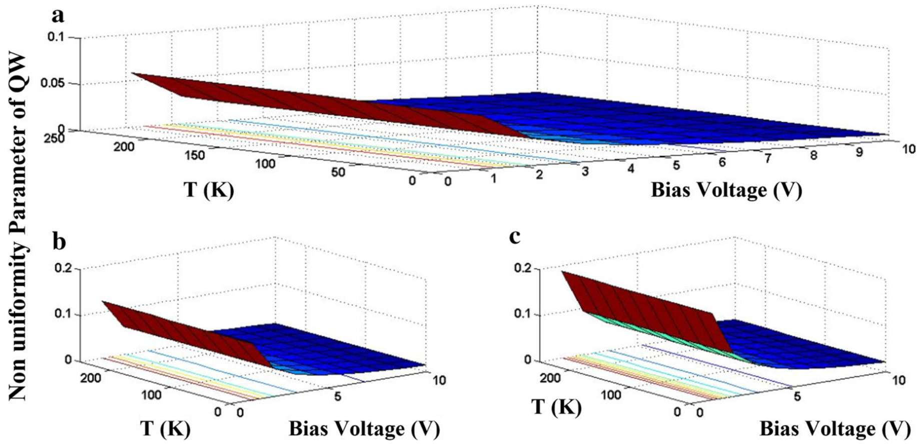

Fig. 7 The nonuniformity parameter distribution of QW base against bias voltage and operating temperature at different ionizing energy with **a** 5 meV, **b** 10 meV, **c** 15 meV

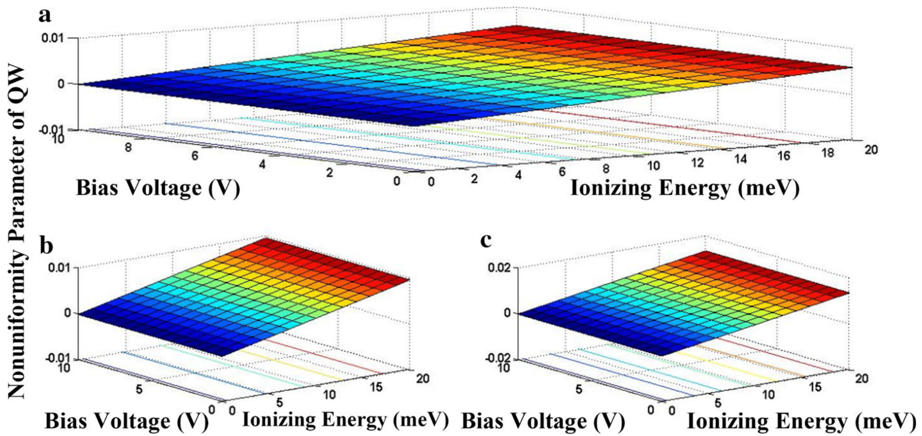

Fig. 8 The nonuniformity parameter distribution of QW base against ionizing energy and bias voltage at different values of the spacing between QWs of **a** 15 nm, **b** 25 nm, **c** 35 nm

smaller number of excited electrons from the QRs on the device uniformity less than the applied potential. Figures 11 and 12 show the change of nonuniformity parameter distribution of QR against temperature at different number of QR sheet layers and number of carriers occupied by each QR, respectively. The obtained results of these figures confirm

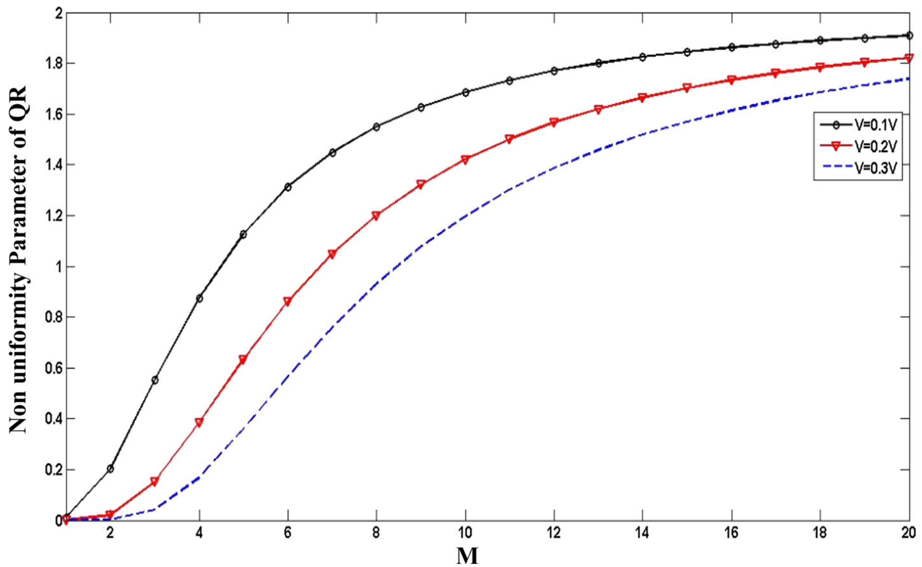

Fig. 9 The nonuniformity parameter distribution of QR base against number of QR sheet layers at different biasing voltage in QR structure with $C_5 = 0.1$, $N_{QR} = 10$, æ = 12, $a_{QR} = 10$ nm, $\Sigma_{QR} = 10^6$ cm^{-2} and $P_0 = 0.02$

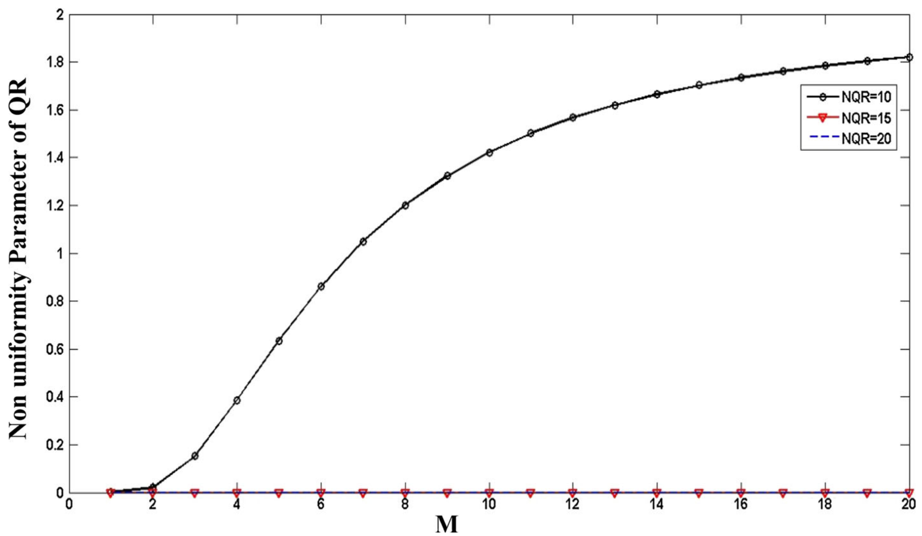

Fig. 10 The nonuniformity parameter distribution of QR base against number of QR sheet layers at different number of carriers occupied by each QR with T = 100 K, V = 0.2 V, æ = 12, $\rho_D = 10^{12}$ and $\Sigma_{QR} = 10^6$ cm^{-2}

that the nonuniformity does not influenced by low temperature. The threshold temperature is found to be 80 K under various parameters values. However, the nonuniformity distribution increases with temperature. It is observed that the temperature increases the thermionic excitations. Hence, the potential distribution within QRs by bias voltage

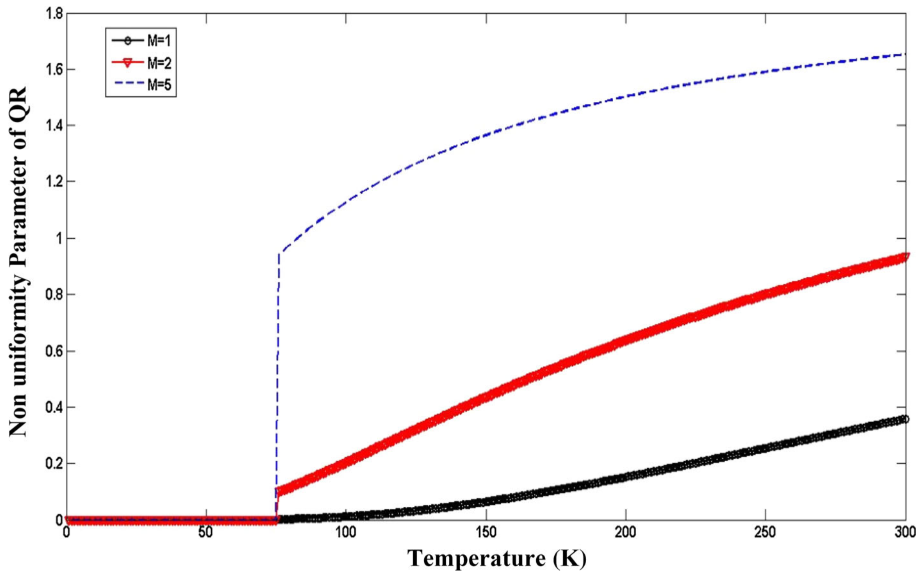

Fig. 11 The nonuniformity parameter distribution of QR base against temperature at different number of QR sheet layers with V = 0.1 V, $N_{QR} = 10$, $a_{QR} = 10$ nm, $\rho = 10^{10}$ cm^{-2} and $C_5 = 0.1$

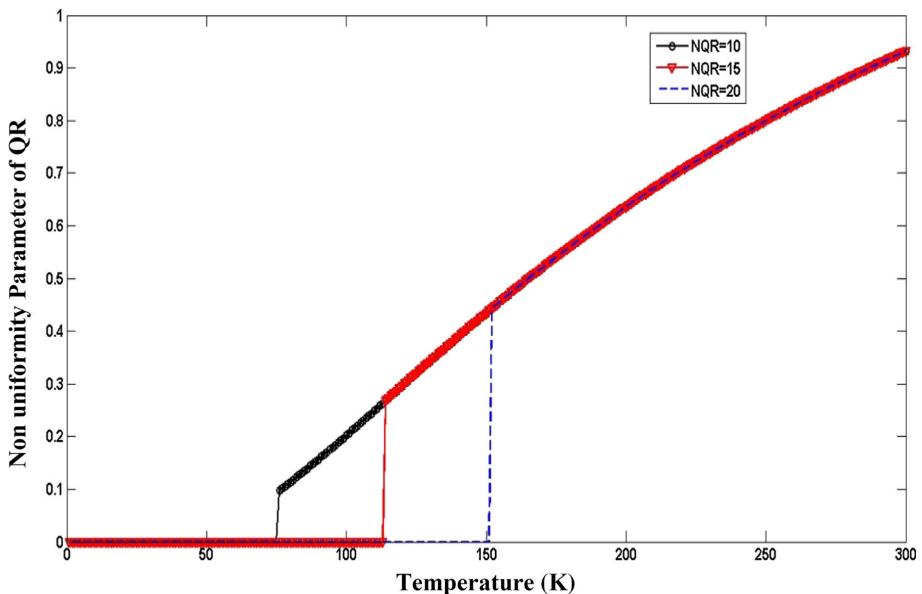

Fig. 12 The nonuniformity parameter distribution of QR base against temperature at different number of carriers occupied by each QR with M = 2, V = 0.1 V, $a_{QR} = 10$ nm and $\rho = 10^{10}$ cm^{-2}

cancels the excited electrons. Consequently, the nonuniformity distribution increases with temperature. After threshold temperature of 80 K, the nonuniformity starts to suddenly rise up depending on the number of QR sheet layers as demonstrated in Fig. 11. Then, the

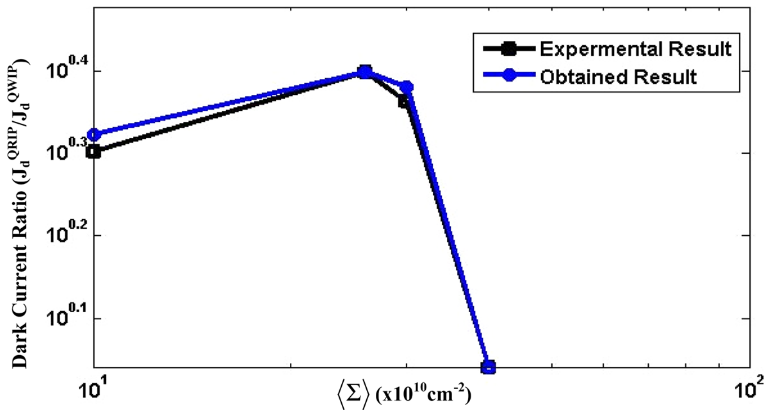

Fig. 13 Dark current ratio (J_d^{QRIP}/J_d^{QWIP}) against average electron sheet density with æ = 12, $N_{QR} = 10$, $a_{QR} = 20$ nm, $\beta_{QRIP} = 0.751$, $\beta_{QWIP} = 0.99$, M = 10, $\Sigma_{QR} = 10^8$ cm^{-2}, $W_e = 100$ nm, $W_c = 100$ nm and T = 60 K

nonuniformity increases smoothly with temperature. On other hand, the nonuniformity increases with number of QR sheet layers. The main reason is the fast increase of electrons thermionic excitation with both temperature and large number of QR sheet layers. Thus, these lead to potential field that modifies the structure uniformity. It is illustrated in Fig. 10 that the structure nonuniformity vanished with higher occupancy of electrons within QR. Therefore, the resistance to overcome the puncture field is higher with N_{QR} as shown in Fig. 12. Hence, the threshold temperature for $N_{QR} = 20$ is 150 K that is larger than a threshold temperature of 80 K at $N_{QR} = 10$. Even though, their effects are identical at higher temperature values. Finally, extension of operating temperature range to be above (150–200) K is the main strength of the proposed models under nonuniformity distribution of QRs.

4.2.2 *Dark current ratio (J_d^{QRIP}/J_d^{QWIP}) results*

The ratio of the dark current densities versus average electron sheet density is depicted in Fig. 13. From this figure, the dark currents ratio (J_d^{QRIP}/J_d^{QWIP}) is introduced by two competitive effects. The first one is lowering of the Fermi energy of the electrons in the QRs (in comparison with the QWs) due to high density of states in the one-dimensional electron. However, the other one intended for the increase of the current density in the regions between the QRs owing to the potential in these regions. Moreover, high agreements between our obtained and published results (Ryzhii et al. 1996) are depicted in Fig. 13. The variation of the dark current ratio (J_d^{QRIP}/J_d^{QWIP}) against number of sheet layers at different longitudinal length of each QRs, temperature and bias voltage are shown in Figs. 14, 15 and 16, respectively. From these figures, the number of thermally excited electrons increases with number of sheet layers. In addition, the probability of electron tunneling between neighboring QRs increases with number of sheet layers. Consequently, the dark current ratio between QRIP and QWIP increases with the number of sheet layers. This process is limited to the saturation that observed in the curves. It is found that optimum number of sheet layers is 5. Also, the dark current ratio increases with the longitudinal length of each QRs as depicted in Fig. 14. The probability of electrons escaping from the wire increases with the longitudinal length of each QRs. Also, the

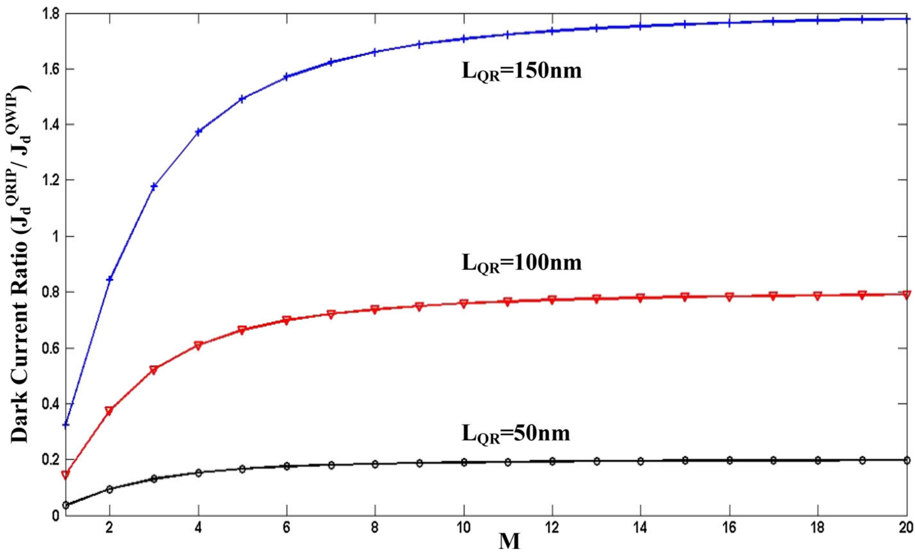

Fig. 14 The dark current ratio (J_d^{QRIP}/J_d^{QWIP}) against number of sheet layers at different longitudinal length of each QRs with $\beta_{QRIP} = 0.751$, $\beta_{QWIP} = 0.99$, $V = 0.1$ V, $N_{QR} = 10$, $a_{QR} = 10$ nm, $\rho = 10^{10}$ and $\rho_D = 10^{12}$ cm^{-2}

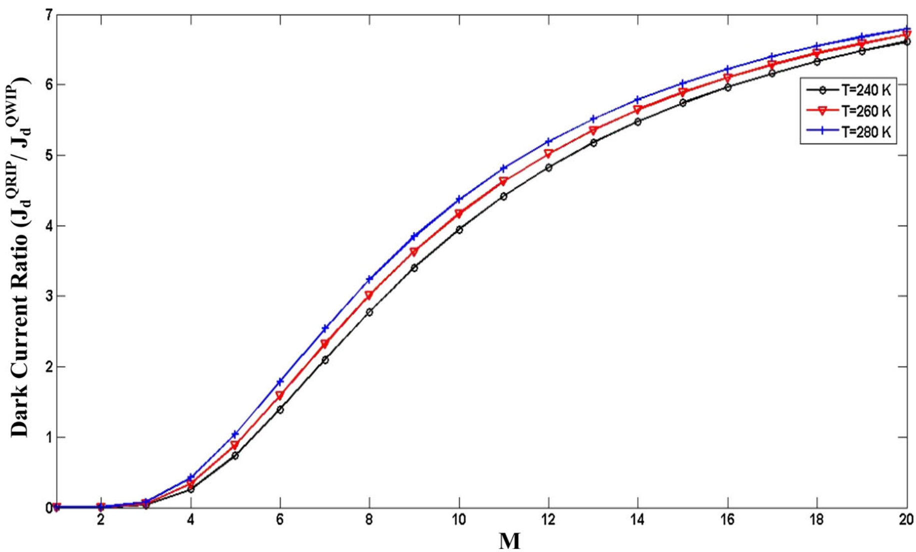

Fig. 15 The dark current ratio (J_d^{QRIP}/J_d^{QWIP}) against number of sheet layers at different temperature with $\beta_{QRIP} = 0.751$, $\beta_{QWIP} = 0.99$, $V = 1$ V, $N_{QR} = 10$, $a_{QR} = 10$ nm, $æ = 12$, $\rho = 10^{10}$ and $\rho_D = 10^{12}$ cm^{-2}

thermal excitations of electron from the QR increase with this length due to free movement of electrons within longitudinal length of each QRs. As expected, the dark current of QRIP device increases with temperature. The high temperature leads to an increase of the thermal

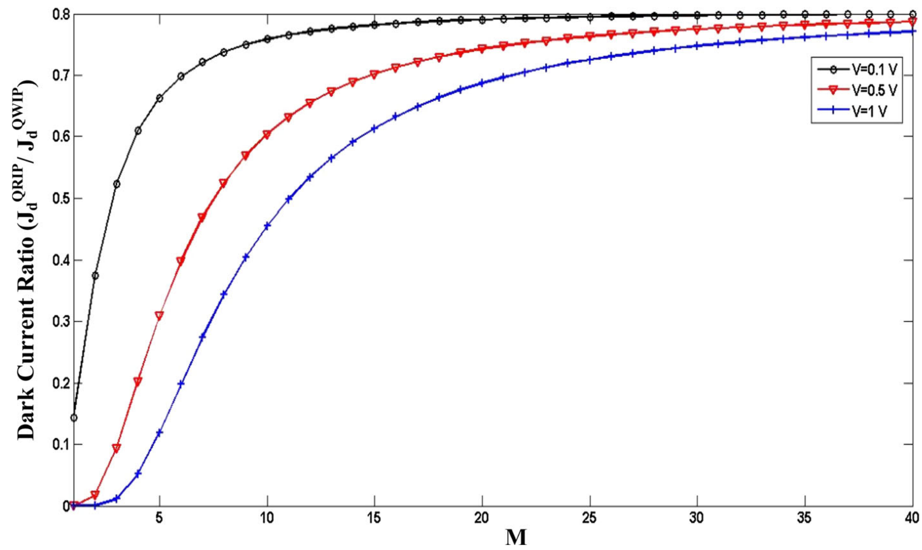

Fig. 16 The dark current ratio (J_d^{QRIP}/J_d^{QWIP}) against number of sheet layers at different bias voltage with $\beta_{QRIP} = 0.751$, $\beta_{QWIP} = 0.99$, $<\Sigma> = 10^{10}$ cm^{-2}, $N_{QR} = 10$, $a_{QR} = 10$ nm, æ = 12, $\rho = 10^{10}$ and $\rho_D = 10^{12}$ cm^{-2}

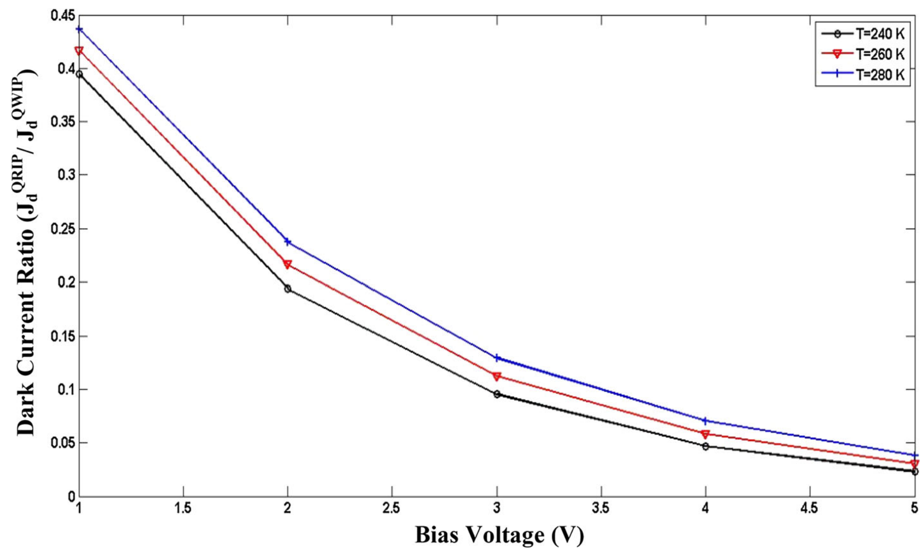

Fig. 17 The dark current ratio (J_d^{QRIP}/J_d^{QWIP}) against bias voltage at different temperature with M = 10, $\beta_{QRIP} = 0.751$, $\beta_{QWIP} = 0.99$, $<\Sigma> = 10^{10}$ cm^{-2}, $N_{QR} = 10$, $a_{QR} = 10$ nm, æ = 12, $\rho = 10^{10}$ and $\rho_D = 10^{12}$ cm^{-2}

excitation of electrons. Also, the tunneling of electrons between adjacent QRs increases with temperature due to excitation energy the electrons receive by temperature. Hence, the dark current ratio (J_d^{QRIP}/J_d^{QWIP}) increases with temperature as illustrated in Fig. 15.

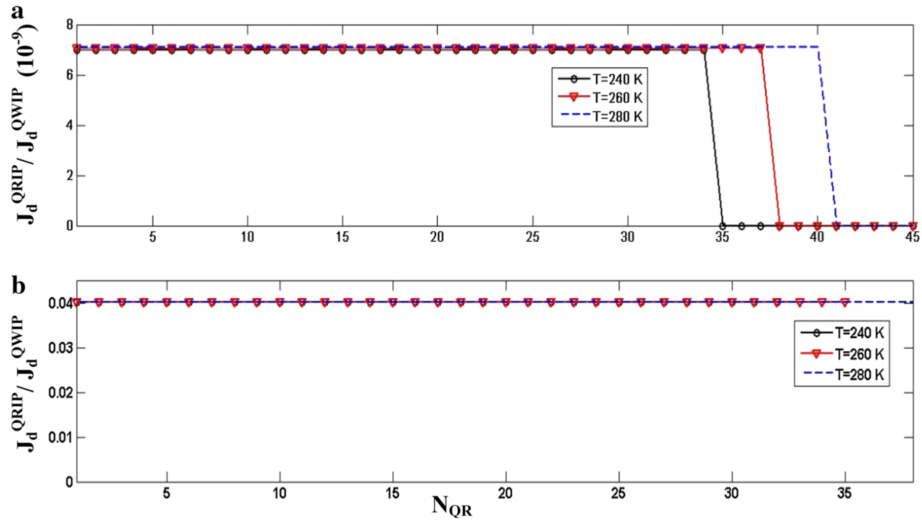

Fig. 18 The dark current ratio (J_d^{QRIP}/J_d^{QWIP}) against against number of carriers occupied by each QR at different temperature under, **a** uniform QR base, **b** nonuniformity QRs base with M = 10, V = 0.2, $\beta_{QRIP} = 0.751$, $\beta_{QWIP} = 0.99$, $<\Sigma> = 10^{10}$ cm^{-2}, $N_{QR} = 10$, $a_{QR} = 10$ nm, æ = 12, $\rho = 10^{10}$ and $\rho_D = 10^{12}$ cm^{-2}

Moreover, the dark current ratio (J_d^{QRIP}/J_d^{QWIP}) decreases with the bias voltage as shown in Fig. 16. It is observed that dark current of QWIP increases with bias voltage due to large injection of electrons from the emitter directed to the QWIP active region. Consequently, the denominator of the dark current ratio (J_d^{QRIP}/J_d^{QWIP}) increases. Thus, this ratio (J_d^{QRIP}/J_d^{QWIP}) decreases. The change of dark current ratio (J_d^{QRIP}/J_d^{QWIP}) against bias voltage at different temperature is shown in Fig. 17. From this figure, the dark current ratio (J_d^{QRIP}/J_d^{QWIP}) decreases with the bias voltage. However, it increases with the temperature as illustrated in Fig. 15.

The variation of dark current ratio (J_d^{QRIP}/J_d^{QWIP}) against number of carriers occupied by each QR at different temperature under uniformity and nonuniformity distribution of QRs is illustrated in Fig. 18. It is observed that the dark current ratio (J_d^{QRIP}/J_d^{QWIP}) remains constant at small number of carriers occupied by each QR. This ratio is vanished at large number of carriers occupied by each QR under uniformity distribution of QRs. The threshold number of carriers occupied by each QR is found to be 35, 38 and 41 at corresponding temperature values of 240, 260 and 280 K. The obtained results show that the threshold value depends on the temperature variation. However, this ratio is canceled at the corresponding number of carriers occupied by each QR under nonuniformity distribution of QRs. Moreover, it is noted that smaller dark current ratio is achieved under uniformity QRs distribution compared to nonuniformity distribution of QRs. The dark current ratio (J_d^{QRIP}/J_d^{QWIP}) against temperature at different lateral characteristic size of QR under uniform QR and nonuniformity QRs is depicted in Fig. 19. From this figure, the dark current ratio is vanished at low temperature values. However, a threshold temperature of 200 K changes the behaviors of dark current ratio. It suddenly increases under both uniformity and nonuniformity distribution of QRs base. Then, it increases smoothly with temperature. It is noted that lateral characteristic size of QR has no effect on the obtained curves. Moreover, the dark current ratio under uniformity distribution is lower than that of nonuniformity QRs distribution.

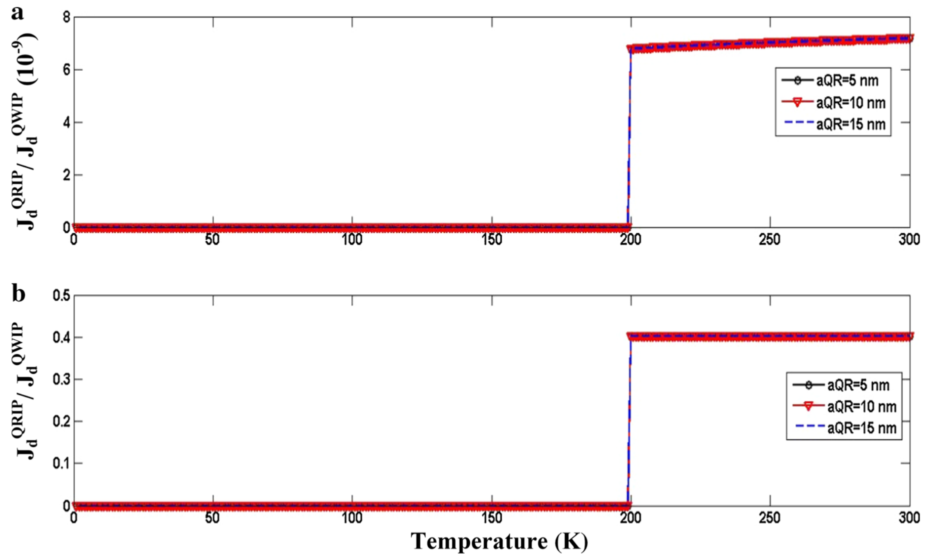

Fig. 19 The dark current ratio (J_d^{QRIP}/J_d^{QWIP}) against temperature at different lateral characteristic size of QR under, **a** uniform QR base, **b** nonuniformity QRs base with V = 0.2 V, N_{QR} = 10, β_{QRIP} = 0.751, β_{QWIP} = 0.99, $<\Sigma>$ = 10^{10} cm^{-2} and M = 10

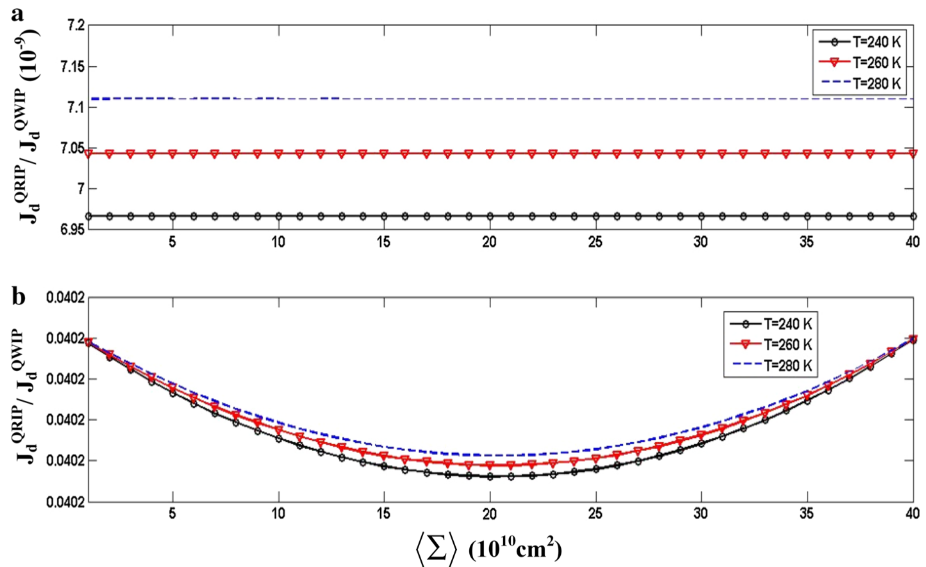

Fig. 20 The dark current ratio (J_d^{QRIP}/J_d^{QWIP}) against average electron sheet density for the undoped QR base at temperature under, **a** uniform QR base, **b** nonuniformity QRs base with V = 0.2 V, M = 10, N_{QR} = 10 and a_{QR} = 10 nm

The variation of dark current ratio (J_d^{QRIP}/J_d^{QWIP}) against average electron sheet density for the undoped QR base at temperature under uniformity QR and nonuniformity QRs is shown in Fig. 20. It is discussed above that dark current ratio increases with temperature

under both uniformity and nonuniformity QRs distribution. Also, this ratio remains constant at low and high average electron sheet density for the undoped QR base under uniformity distribution. Though, this ratio decreases with average electron sheet density for the undoped QR base until a threshold limit of 20×10^{10} cm^2. This may be due to the decrease of dark current with radiative recombination of the carriers in the active region. Then, the dark current ratio starts to increase with average electron sheet density for the undoped QR base due to the increase of thermal excitation of carriers that rises with average electron sheet density. Also, the dark current ratio under uniformity distribution is lower than that of nonuniformity QRs distribution. The obtained results confirm the importance of uniformity distribution of QRs on the dark current of QRIP device.

The variation of dark current ratio (J_d^{QRIP}/J_d^{QWIP}) with operating temperature at different values of nonuniformity parameter is depicted in Fig. 21. The theoretical result demonstrates that no dark current is observed at all for zero value of ψ as shown in Fig. 21a that not found practically. But, the dark current ratio stills small for $\psi \leq 1$ as illustrated in Fig. 21b, c. It is noted that the dark current of QWIP is more sensitive to the nonuniformity parameter. Hence, the dark current of QWIP is much higher than dark current of QRIP. Therefore, the dark current ratio is found to be smaller than expected. However, the dark current of QRIP increases with the increase of ψ to be above unity as shown Fig. 21d. Also, the 3D change of dark current ratio (J_d^{QRIP}/J_d^{QWIP}) with operating temperature and average electron sheet density at different nonuniformity parameter values is depicted in Fig. 22. This figure shows the 3D variation of dark current ratio (J_d^{QRIP}/J_d^{QWIP}) under effects of nonuniformity distribution with $\psi < 1$, $\psi = 1$ and $\psi > 1$ as shown in Fig. 22a–c, respectively. Consequently, the dark current ratio increase to some extent depending on the nonuniformity parameter value. Thus, the nonuniformity distribution parameter corresponds to 1 under uniform distribution of QWs and QRs. This parameter is greater than unity under a large variation of nonuniformity distribution. However, it is smaller than unity at small variation of nonuniform distribution. Finally, the zero value of this parameter enhances the optical properties of the underlined structures. Since, no dark current is observed. Consequently, these results demonstrate the potential effects of the

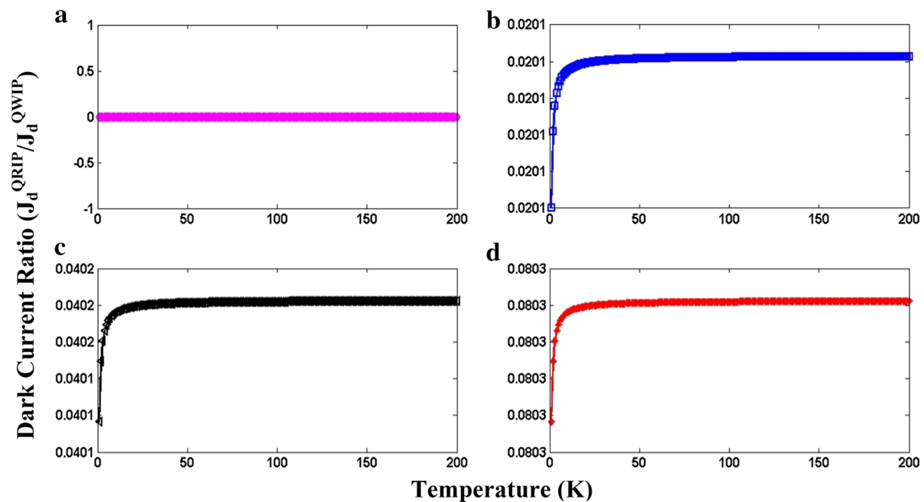

Fig. 21 Dark current ratio (J_d^{QRIP}/J_d^{QWIP}) against operating temperature at different non uniformity distribution values with **a** $\psi = 0$, **b** $\psi = 0.5$, **c** $\psi = 1$, **d** $\psi = 2$

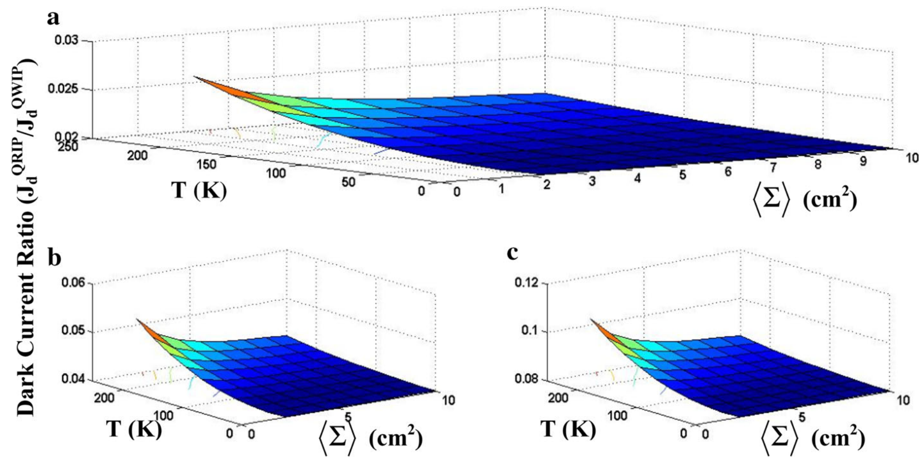

Fig. 22 The 3D variation of dark current ratio (J_d^{QRIP}/J_d^{QWIP}) against operating temperature and average electron sheet density at different non uniformity distribution values with **a** $\psi = 0.5$, **b** $\psi = 1$, **c** $\psi = 2$

nonuniformity distribution on QWIP and QRIP structures. As a last point of observation, the dark current of QRIPs is greater than the dark current of QWIP structures under large variation of the nonuniformity parameter.

5 Conclusion

The performances of QWIP and QRIP are investigated under uniformity and nonuniformity distribution of QWs/QRs base. The dark current of QWIP and QRIP devices are estimated with special emphasis on the nonuniformity distribution of QWs and QRs. Therefore, the aim of the manuscript is to reduce the dark current of quantum photodetectors under uniformity and nonuniformity distribution of QWs and QRs for far infrared photodetectors. Moreover, the dark current density ratio between QRIP and QWIP is considered. The optimum performance of underlined devices is achieved. Subsequently, the optimum parameters values of QWIP are obtained using number of QW layers of 10, separation between QW of 9.7 nm and average sheet electron density in the QW in equilibrium of 0.63×10^{11} cm^{-2}. In addition, the optimum behavior is perceived with QR sheet electron density of 20×10^{10} cm^{2}. Furthermore, the obtained results are compared with literature results and good agreement is introduced. The influences of nonuniformity distribution of QWs and QRs on dark current of IR photodetectors are investigated. It is concluded that nonuniformity distribution effect is reduced with the number of carriers occupied by each QR. Also, this factor is diminished by applied bias voltage. The proposed work confirms that the temperature range can be extended to (150–200) K using higher number of carriers occupied by each QRs. However, this current ratio is observed to suddenly increase above 200 K. It is noted that lateral characteristic size of QR has no effect on the dark current ratio. As a final point of observation, the dark current ratio increases with the number of sheet layers and longitudinal length of each QRs due to increase of QRIP dark current. Therefore, the device performance is improved. Consequently, the operations of underlined infrared photodetectors are robust against noise sources in FIR spectrum. Hence, the operation of QWIP and QRIP devices can be extended in FIR spectrum region.

References

Altin, E., Hostut, M., Ergun, Y.: Dark current and optical properties in asymmetric GaAs/AlGaAs staircase-like multiquantum well structure. Infrared Phys. Technol. **58**, 74–79 (2013)

Bai, H., Zhang, J., Wang, X., Liu, X.: Characteristics analysis of dark current in quantum dot infrared photodetectors. Opt. Laser Technol. **48**, 337–342 (2013)

Barickaby, H., Zarifkar, A., Sheikhi, M.H.: A new approach for modeling of dark current characteristics of quantum wire infrared photodetectors. Optoelectron. Lett. **7**(4), 0260–0262 (2011)

Castellano, F., Iotti, R.C., Rossi, F., Faist, J., Lhuillier, E., Berger, V.: Modeling of dark current in mid-infrared quantum-well infrared photodetectors. Infrared Phys. Technol. **52**, 220–223 (2009)

de Moura Pedroso, D., Vieira, G.S., Passaro, A.: Modelling of high-temperature dark current in multi-quantum well structures from MWIR to VLWIR. Phys. E **86**, 190–197 (2017)

DeCuir Jr., E.A., Choi, K.-K., Sun, J., Wijewarnasuriya, P.S.: Progress in resonator quantum well infrared photodetector (R-QWIP) focal plane arrays. Infrared Phys. Technol. **70**, 138–146 (2015)

El_Tokhy, M.S., Mahmoud, I.I.: Performance evaluation of quantum well infrared phototransistor instrumentation through modeling. Opt. Eng. **53**(5), 054104-1–054104-11 (2014)

El_Tokhy, M.S., Mahmoud, I.I.: Performance analysis of PIN photodiode under gamma radiation effects through modeling. J. Opt. **44**(4), 353–365 (2015)

El_Tokhy, M.S., Mahmoud, I.I., Konber, H.A.: Comparative study between different quantum infrared photodetectors. Opt. Quantum Electron. **41**(11), 933–956 (2009)

El_Tokhy, M.S., Mahmoud, I.I., Konber, H.A.: Performance improvement of quantum well infrared photodetectors through modeling. J. Naophotonics **4**, 043518-1–043518-15 (2010a)

El_Tokhy, M.S., Mahmoud, I.I., Konber, H.A.: Characteristics analysis of quantum wire infrared photodetectors under both dark and illumination conditions. Infrared Phys. Technol. **53**(5), 320–335 (2010b)

Ershov, M., Liu, H.C., Perera, A.G.U., Matsik, S.G.: Optical interference and nonlinearities in quantum-well infrared photodetectors. Phys. E **7**, 115–119 (2000)

Etteh, N.E.I., Harrison, P.: The role of sequential tunnelling in the dark current of quantum well infrared photodetectors (QWIPs). Superlattices Microstruct. **30**(5), 273–278 (2001)

Etteh, N.E.I., Harrison, P.: Quantum mechanical scattering investigation of the dark current in quantum well infrared photodetectors (QWIPs). Infrared Phys. Technol. **44**, 473–480 (2003)

Goldberg, A., Choi, K.K., Cho, E., McQuiston, B.: Laboratory and field performance of megapixel QWIP focal plane arrays. Infrared Phys. Technol. **47**, 91–105 (2005)

Guériaux, V., Nedelcu, A., Carras, M., Huet, O., Marcadet, X., Bois, P.: Mid-wave QWIPs for the [3–4.2 μm] atmospheric window. Infrared Phys. Technol. **52**, 235–240 (2009)

Gunapala, S.D., Bandara, S.V., Liu, J.K., Mumolo, J.M., Hill, C.J., Rafol, S.B., Salazar, D., Woolaway, J., LeVan, P.D., Tidrow, M.Z.: Towards dualband megapixel QWIP focal plane arrays. Infrared Phys. Technol. **50**, 217–226 (2007a)

Gunapala, S.D., Bandara, S.V., Hill, C.J., Ting, D.Z., Liu, J.K., Rafol, S.B., Blazejewski, E.R., Mumolo, J.M., Keo, S.A., Krishna, S., Chang, Y.-C., Shott, C.A.: Demonstration of 640 × 512 pixels long-wavelength infrared (LWIR) quantum dot infrared photodetector (QDIP) imaging focal plane array. Infrared Phys. Technol. **50**, 149–155 (2007b)

Gunapala, S.D., Bandara, S.V., Liu, J.K., Mumolo, J.M., Ting, D.Z., Hill, C.J., Nguyen, J., Simolon, B., Woolaway, J., Wang, S.C., Li, W., LeVan, P.D., Tidrow, M.Z.: 1024 × 1024 Format pixel co-located simultaneously readable dual-band QWIP focal plane. Infrared Phys. Technol. **52**, 395–398 (2009)

Hansson, C., Rachavula, K.K.: Comparative study of infrared photodetectors based on quantum wells (QWIPS) and quantum dots (QDIPS). Master's Thesis, Halmstad University (2006)

Kuffner, P.: Quantum dot interdiffusion for two colour quantum dot infrared photodetectors. A Thesis Submitted as Partial Fulfillment of the Requirements for the Degree of Bachelor of Engineering with Honours at the Australian National University, u3289067 (2006)

Li, N., Xiong, D.-Y., Yang, X.-F., Lu, W., Xu, W.-L., Yang, C.-L., Hou, Y., Fu, Y.: Dark currents of GaAs/AlGaAs quantum-well infrared photodetectors. Appl. Phys. A **89**, 701–705 (2007). doi:10.1007/s00339-007-4142-2

Ling, H.S., Wang, S.Y., Lee, C.P., Lo, M.C.: Confinement-enhanced dots-in-a-well QDIPs with operating temperature over 200 K. Infrared Phys. Technol. **52**, 281–284 (2009)

Liu, H., Yang, C., Zhang, J., Shi, Y.: Detectivity dependence of quantum dot infrared photodetectors on temperature. Infrared Phys. Technol. **60**, 365–370 (2013)

Liu, G., Zhang, J., Wang, L.: Dark current model and characteristics of quantum dot infrared photodetectors. Infrared Phys. Technol. **73**, 36–40 (2015)

Martyniuk, P., Rogalski, A.: Quantum-dot infrared photodetectors: status and outlook. Prog. Quantum Electron. **32**, 89–120 (2008)

Matsukura, Y., Uchiyama, Y., Yamashita, H., Nishino, H., Fujii, T.: Responsivity–dark current relationship of quantum dot infrared photodetectors (QDIPs). Infrared Phys. Technol. **52**, 257–259 (2009)

Meola, C., Boccardi, S., Carlomagno, G.M.: Measurements of very small temperature variations with LWIR QWIP infrared camera. Infrared Phys. Technol. **72**, 195–203 (2015)

Mitin, V., Sergeev, A., Vagidov, N., Birner, S.: Improvement of QDIP performance due to quantum dots with built-in charge. Infrared Phys. Technol. **59**, 84–88 (2013)

Negi, C.M.S., Kumar, J.: Investigation of p-type multicolour-broadband quantum dot infrared photodetector. Superlattices Microstruct. **82**, 336–348 (2015)

Ryzhii, V.: Characteristics of quantum well infrared photodetectors. J. Appl. Phys. **81**, 6442–6448 (1997). doi:10.1063/1.364426

Ryzhii, V., Liu, H.C.: Contact and space-charge effects in quantum well infrared photodetectors. Jpn. J. Appl. Phys. **38**, 5815–5822 (1999)

Ryzhii, V., Ryzhii, M.: Nonlinear dynamics of recharging processes in multiple quantum well structures excited by infrared radiation. Phys. Rev. B **62**, 10292–10296 (2000). doi:10.1103/PhysRevB.62.10292

Ryzhii, V., Khmyrova, I., Ershov, M., Lizuka, T.: Theory of an intersubband infrared phototransistor with a uniform quantum well. Semicond. Sci. Technol. **10**, 997–1001 (1995). doi:10.1088/0268-1242/10/7/016

Ryzhii, V., Khmyrova, I., Ryzhii, M., Ershov, M.: Comparison studies of infrared phototransistors with a quantum-well and a quantum-wire base. J. Phys. IV **6**, C3-157–C3-161 (1996). doi:10.1051/jp4:1996324

Ryzhii, M., Ryzhii, V., Willander, M.: Effect of donor space charge on electron capture processes in quantum well infrared photodetector. Jpn. J. Appl. Phys. **38**, 6650–6653 (1999)

Ryzhii, M., Ryzhii, V., Suris, R., Hamaguchi, C.: Periodic electric-field domains in optically excited multiple-quantum-well structures. Phys. Rev. B **61**(4), 2742–2748 (2000a)

Ryzhii, V., Khmyrova, I., Ryzhii, M., Suris, R., Hamaguchi, C.: Phenomenological theory of electric-field domains induced by infrared radiation in multiple quantum well structures. Phys. Rev. B **62**, 7268–7274 (2000b). doi:10.1103/PhysRevB.62.7268

Soibel, A., Bandara, S.V., Ting, D.Z., Liu, J.K., Mumolo, J.M., Rafol, S.B., Johnson, W.R., Wilson, D.W., Gunapala, S.D.: A super-pixel QWIP focal plane array for imaging multiple waveband temperature sensor. Infrared Phys. Technol. **52**, 403–407 (2009)

Wang, S.Y., Lee, C.P.: Nonuniform quantum well infrared photodetectors. J. Appl. Phys. **87**(522), 522–525 (2000). doi:10.1063/1.371893

Wang, S.Y., Chin, Y.C., Lee, C.P.: A detailed study of non-uniform quantum well infrared photodetector. Infrared Phys. Technol. **42**, 177–184 (2001)

Wang, S.Y., Ling, H.S., Lo, M.C., Lee, C.P.: Detection wavelength and device performance tuning of InAs QDIPs with thin AlGaAs layers. Infrared Phys. Technol. **52**, 264–267 (2009)